ACS APPLIED MATERIALS & INTERFACES

RESEARCH ARTICLE

www.acsami.org

Biocompatible Carbohydrate-Functionalized Stainless Steel Surfaces: A New Method For Passivating Biomedical Implants

Anne M. Slaney,[†,§] Vincent A. Wright,[†,§] Peter J. Meloncelli,[‡,§] Kenneth D. Harris,[†] Lori J. West,[⊥] Todd L. Lowary,[*,‡,§] and Jillian M. Buriak[*,†,§]

[†]NRC National Institute for Nanotechnology, [‡]Alberta Ingenuity Centre for Carbohydrate Science, [§]Department of Chemistry, and [⊥]Faculty of Medicine and Dentistry, University of Alberta, Edmonton, Alberta T6G 2G2, Canada

Supporting Information

ABSTRACT: A convenient method for passivating and functionalizing stainless steel is described. Several methods of coating stainless steel (SS) samples with silica were investigated and of these methods, a thin (less than 15 nm thick) layer of silica created by atomic layer deposition (ALD) was found to give superior performance in electrochemical testing. These interfaces were then used as a platform for further functionalization with molecules of biological interest. Specifically, the SS samples were functionalized with biologically significant carbohydrates [*N*-acetyl-D-glucosamine (GlcNAc) and D-galactose (Gal)] that contain trialkoxysilane derivatives as chemical handles for linking to the surface. The presence and biological availability of these moieties on the silica coated SS were confirmed by XPS analysis and an enzyme-linked lectin assay (ELLA) using complementary lectins that specifically recognize the surface-bound carbohydrate. This method has the potential of being adapted to the functionalization of stainless steel biomedical implants with other biologically relevant carbohydrates.

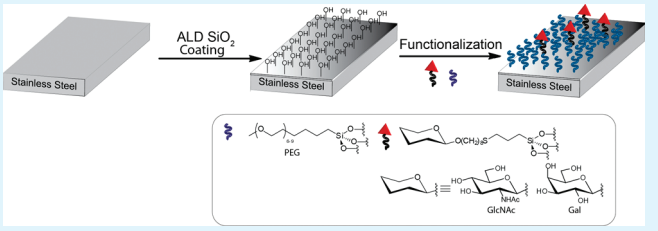

KEYWORDS: 316L stainless steel, atomic layer deposition, silica coating, trialkoxysilane surface functionalization, poly(ethylene glycol), carbohydrate

INTRODUCTION

Implanted biomedical devices, including stents, play important roles in alleviating morbidity, improving the quality of life and prolonging longevity of recipient patients with a variety of medical conditions. About 1.4 million stents are implanted annually worldwide, typically as part of a treatment to maintain patency of the vascular system.[1] Essential to the function of these devices is the selection of an appropriate structural material; metals are often the material of choice over ceramics and polymers because of their superior mechanical properties such as malleability and shape retention.[2−7] In addition to physical requirements such as flexibility and strength,[4,5] implanted biomedical devices must have appropriate chemical properties, most notably sufficient chemical inertness to exist indefinitely in the corrosive environment of high salinity human body fluids without undergoing substantial release of degradation products.[8−11] Only a few common metals and alloys meet these prerequisites, and thus the majority of biomedical implants comprise such materials, most notably titanium and its alloys, Co−Cr alloys, and stainless steels,[12,13] with 316L stainless steel being the most widely used because of cost considerations.[2,5,14,15]

As the majority of coronary stents approved by the U.S. Food and Drug Administration are fabricated from stainless steel,[5,14,16] its surface chemistry and subsequent functionalization are critical to successful implementation. Stainless steel is an iron alloy that contains at least 12% chromium and often other transition metals.[8,12,27] Chromium incorporation results in the spontaneous formation of a chromium oxide rich surface layer, approximately 5−10 nm thick depending on the surrounding environment.[11,28,29] This passivating metal oxide inhibits further oxidation of the bulk metal and is the source of the corrosion resistance of stainless steel.[28] American Iron and Steel Institute (AISI) 316L stainless steel is a low carbon content iron alloy containing 16−18.5% Cr, 10−14% Ni, and 2−3% Mo, that is frequently used in biomedical devices due to its corrosion resistance in aqueous environments.[12] This material will be used for all experiments in this paper.

The oxide passivation layer is vitally important to in vivo biocompatibility because several of the solubilized corrosion byproducts of stainless steel alloys, such as chromium, molybdenum, and nickel ions, have a number of deleterious effects.[9,30] These ions are cytotoxic in high concentrations,[31] suspected carcinogens,[31−33] and suspected allergens.[1,9] Released metal ions[34,35] are problematic as immune responses to metal implants are often observed,[10,36] including restenosis in cardiovascular stents.[1] Furthermore, proteins that immediately adsorb onto the surface can cascade into thrombus or blood clot formation in some instances. An intricate combination of factors is involved in implant thrombogenicity, including surface energy, texture and

Received: February 4, 2011
Accepted: March 28, 2011
Published: March 28, 2011

morphology, and net electrical charge.[5,37−41] Manipulating these factors is, therefore, vital in understanding and enhancing the biocompatibility of implanted devices.

To improve the hemocompatibility and functionality of unmodified stainless steel implants, researchers have devoted substantial attention toward controlling their surface properties.[15,42] Considerable enhancements and improvements with regards to thrombogenicity and other characteristics have been observed through the tailoring of the composition of the natural passivation layer, and the building of functional monolayers on top of this interface.[43−50] However, another widespread approach has been to bypass the direction functionalization of stainless steel and instead, coat the stainless steel surface with a secondary passivation layer, followed by a subsequent termination to attain the desired set of final properties.[15,51−63] Examples where intermediate interfacial layers were used to improve polymer-coating adhesion and tailor the surface characteristics include low-surface-energy polymer films on coronary stents,[2,5,15] as well as self-assembled monolayers (SAM) of organophosphates,[64] thiols,[52,65] and amines.[53] Other interesting approaches include treatment with diazonium salts,[54,66] electrografting of polyacrylate chains,[55−57,67,68] and the application of ceramic coatings.[58,59]

In this work, we describe a general and all-purpose approach for the functionalization of stainless steel surfaces for in vivo applications. We investigate thin (sub-15 nm) and conformal silica coatings deposited by atomic layer deposition (ALD) as a hydroxy-rich interlayer on stainless steel. These ALD coatings act as a platform on which alkoxysilane chemistry can take place. Because of the ubiquity of chloro- and alkoxysilane coupling to hydroxy-terminated surfaces, application of this chemistry to stainless steel substrates could lead to a robust and general set of reaction conditions that allow attachment of a broad range of organic surface terminations to stainless steel. Two biologically relevant carbohydrate moieties were chosen for these studies, *N*-acetyl-D-glucosamine (GlcNAc) and D-galactose (Gal) to demonstrate the versatility and utility of the resulting materials. The selection of these two carbohydrates was based on the plethora of literature on the detection of GlcNAc and Gal functionalized surfaces using the enzyme-linked lectin assay (ELLA).[69−72] We anticipate that this conjugation methodology has broad application to other biologically relevant carbohydrates.

MATERIALS AND METHODS

Materials. Unless otherwise indicated, all materials were used as received. Nitric acid, hydrofluoric acid and sulphuric acid were purchased from J. T. Baker; hydrogen peroxide (ACS grade, 30%), methylene chloride and acetone from Fischer Scientific; glacial acetic acid, sodium chloride (ACS grade), magnesium chloride hexahydrate (ACS grade), potassium chloride (ACS grade), calcium chloride (anhydrous), and sodium bicarbonate (ACS grade) from EMD; 100% ethanol from Commercial Alcohols; $Ru(III)(NH_3)_6Cl_3$ from Strem-Chemicals; and tetraethyl orthosilicate (reagent grade, 98%), 3-mercaptopropyl trimethoxysilane (MPTMS), 1,2-bis(trimethoxylsilyl)ethane and potassium chloride (99.999%) from Aldrich. 2-[Methoxy(polyethyleneoxy)propyl]-trimethoxysilane (6−9 or 9−12 ethylene glycol repeat units; called alkoxysilane PEG or alkoxysilane PEG (9−12) hereafter) was purchased from Gelest Inc. Eighteen MΩ·cm (Barnstead) water was freshly generated before use. Annealed, 0.9 mm thick, mirror polished both sides stainless steel AISI 316L stainless steel (Fe/Cr18/Ni10/Mo3) foil was purchased from Goodfellow Cambridge Limited.

Biological Assays. PBST refers to a phosphate buffer saline at pH 7.4, containing 0.1% Tween-20. Phosphate buffer saline consists of a solution of 137 mM NaCl, 2.7 mM KCl, 100 mM Na_2HPO_4, and 2 mM KH_2PO_4 in deionized 18 MΩ·cm water. The *o*-phenylenediamine-(OPD) indicator was purchased from Aldrich (SIGMA*FAST* OPD P9187) and prepared according to the manufacturer's instructions. Peanut agglutinin peroxidase conjugate (L7759) and wheat germ agglutinin peroxidase conjugate (L3892) were purchased from Aldrich. Absorbance was measured at 450 nm on a Molecular Devices SPECTRAmax 340PC UV/vis spectrophotometer.

METHODS

Preparation of 316L Stainless Steel Coupons. The 0.9 mm thick mirror-polished 316L stainless steel coupon was extensively rinsed with chloroform, ethanol, and pentane before being cut into 1 cm × 1 cm pieces with a press. Prior to silica deposition or alkoxysilane surface functionalization, all samples were ultrasonically cleaned for 10 min in each of four solvents (18 MΩ·cm H_2O, CH_2Cl_2, acetone, ethanol). The cleaned pieces were dried under a stream of nitrogen and immediately treated with air plasma[47] for 60 min at a pressure of ∼800 mTorr (Harrick Plasma, PDC32G, 18 W).

Dip Coating of Silica on 316L Stainless Steel Surfaces. In general, upon removal from the plasma cleaner, the stainless steel coupon was kept in freshly generated 18 MΩ·cm H_2O until it was adhered to a glass slide with adhesive putty, such that six samples could be prepared in tandem. Adhesive putty was used as it was found to leave less residue than glue, varnish, or tape. The steel face in contact with the adhesive putty remained unexposed to all chemical processing such that unimpeded electrical contact could be made with this face. The glass slide with six samples was immersed in silica precursor solution for 15 s. The silica precursor solution varied from neat TEOS[60] to ethanol (100% or 95%) solutions of TEOS, or lower pH-adjusted (1% acetic acid v/v 95% ethanol) ethanolic solutions. Upon withdrawal, the edge of the samples was dabbed on a Kimwipe to remove excess silica precursor solution. In all methods except one,[60] the sample was then cured for 15 min at 110 °C, completing a cycle. Subsequently, samples were immersed in 18 MΩ·cm H_2O for 5 min and dried under nitrogen prior to being immersed in the silica precursor solution to commence the second cycle. Typically five cycles were performed. Following the dip procedure, the sample side exposed to the adhesive putty was rinsed with water, toluene, pentane, dichloromethane, acetonitrile, acetone and ethanol before drying in air for 24 h at room temperature. Alternatively, the glass slide with the six samples was immediately immersed in a 2% v/v silane (1,2-bistrimethoxysilylethane or alkoxysilane PEG) solution in acidic ethanol (95% ethanol, 1% acetic acid v/v) and gently agitated for 2 min. The silane solution was prepared 15 min before use to allow the alkoxysilane groups to hydrolyze to silanol groups. Upon withdrawal from the silane solution, the samples were briefly dipped in 100% ethanol, before being cured for 15 min in an oven heated to 110 °C. Following the dip procedure, the sample side exposed to the adhesive putty was rinsed with water, toluene, pentane, dichloromethane, acetonitrile, acetone and ethanol before drying in air for 24 h at room temperature.

Electrodeposition of Silica Coatings on 316L Stainless Steel Surfaces. A sol−gel solution was prepared according to a slight modification of a literature procedure.[73] A solution that consisted of 1.0 mL of TEOS or 1.0 mL of alkoxysilane PEG (9−12), 6.5 mL of ethanol, and 2.5 mL of 0.1 M HCl were stirred for at least three hours before use. The sol−gel solution remained translucent for more than one month. A 1.5 cm × 1.5 cm 316L stainless steel coupon with 1.54 cm^2 exposed via a Teflon cell was the working electrode. Heavy aluminum foil was used to make electrical contact with the back side of the stainless steel sample. A platinum wire was used as a counter electrode, and Ag/

Table 1. Concentration of Silanes Used for SS Coupon Functionalization

uncoated SS	ALD silica SS	ALD silica SS
100% PEG	100% PEG	100% PEG
60% PEG/40% GlcNAc	60% PEG/40% GlcNAc	60% PEG/40% Gal
30% PEG/70% GlcNAc	30% PEG/70% GlcNAc	30% PEG/70% Gal
0% PEG/100% GlcNAc	0% PEG/100% GlcNAc	0% PEG/100% Gal

AgCl in saturated KCl was used as a reference electrode. A potential of −1 V was applied for 60 s, while the current was monitored. Upon removal from the electrochemical cell, the stainless steel sample was rinsed with methanol and left to air-dry for 24 h. The sample was then cured for 24 h in an oven heated to 110 °C.

Atomic Layer Deposition of Silica Coatings on 316L Stainless Steel Surfaces. Freshly cleaned stainless steel samples were placed in an Oxford Industries FlexAL atomic layer deposition apparatus. For samples to be electrochemically examined, silica was deposited on one side of the 1 cm × 1 cm stainless steel sample, whereas for samples that were to be functionalized and examined via bioassay, silica was first deposited on one side of a 2 mm × 5 mm sample, then the sample was flipped, and a second identical ALD process was completed on the second side. During deposition, the substrates were maintained at a temperature of 300 °C, and 40 sccm of oxygen were continuously passed through the plasma source. To begin the process, the ALD chamber was first evacuated for 180 s to achieve a base pressure in the range $1-4 \times 10^{-6}$ Torr, followed by several process gas flush and prestabilization steps. The deposition chamber was then repeatedly cycled through a five-step sequence to build up a silica coating of the desired thickness. In each cycle, the chamber was first dosed for 600 ms with bis(tertiarybutylamino)silane (BTBAS) delivered with a 30 sccm flow of argon carrier gas. Excess or loosely bound BTBAS was then removed from the deposition chamber in a 5.5 s purge step using 30 sccm argon at 15 mTorr. Argon flow to the process chamber was then shut down, and the gas environment was allowed to stabilize for 2.5 s at 15 mTorr. A 250 W oxygen plasma was then initiated and maintained for 5 s at 15 mTorr. A second post-plasma argon purge was then performed for 2 s at 15 mTorr, completing the sequence. This process was repeated a specified number of times to produce silica films of the desired thickness. With careful calibration, growth per cycle was determined to be 1.23 Å/cycle (see the Supporting Information, Figure 16), such that a 40 cycle process resulted in the deposition of approximately 5 nm of SiO_2. During every ALD process, a Si(100) witness substrate was included in the deposition chamber, and this witness was examined by variable angle spectroscopic ellipsometry (VASE) in addition to the SiO_2-coated 316L stainless steel samples.

Surface Functionalization: Alkoxysilane Functionalization of 316L Stainless Steel or 5 nm ALD Silica on 316L Stainless Steel Surfaces for Bioassay Examination. In general, the 316L stainless steel 2 mm × 5 mm coupons were cleaned as per the method listed above for the 1 cm × 1 cm coupons. Alternatively, the SiO_2 coated 2 mm × 5 mm 316L stainless steel coupons were cleaned by a 30 s submersion in piranha solution [3:1 concentrated H_2SO_4:30% H_2O_2; ***WARNING**: The preparation of piranha solution is very exothermic, and the mixture reacts violently with organic solvents. Extreme caution should be used when using piranha cleaning solution!*]. The cleaned SiO_2 coated samples were washed with copious amounts of 18 MΩ·cm water and dried under a stream of nitrogen. The freshly cleaned 2 mm × 5 mm 316L stainless steel (whether it be 5 nm ALD silica coated or not) coupons were immediately immersed in a 2% w/w silane with varying concentrations of the monosaccharide **2**/alkoxysilane PEG (Table 1) solution in acidic ethanol (95% ethanol, 1% acetic acid v/v) and gently agitated for 2 min. The silane solution was prepared 15 min before use to allow the alkoxysilane groups to hydrolyze to silanol groups. Upon withdrawal from the silane solution, the sample was briefly dipped in 100% ethanol, before being cured for 15 min in an oven heated to 110 °C.

Surface Characterization. XPS (Kratos Analytical, Axis-Ultra) was performed under a high vacuum ($<1 \times 10^{-8}$ Torr) using monochromatic Al Kα with a photon energy of 1486.6 eV. The spectra were calibrated on the basis of the C 1s peak. Additionally, depth profiling was performed using 4 keV Ar ions, ion current starting at 2 μA. The etched area was 1.5 mm × 1.5 mm and photoelectrons were collected from the center of the etched crater.

Variable angle spectroscopic ellipsometry (VASE) experiments were performed on a J.A. Woollam VASE with HS-190 monochromator. Spectra were recorded in the range 300−1350 nm with data points every 7.5 nm. Signals from 20 complete revolutions of the retarder were averaged for each data point, and spectra were recorded for three incidence angles (47, 57, and 67°). The resulting Ψ and Δ data were fit with a simple model consisting of a Cauchy dielectric including Urbach absorption on a stainless steel substrate.

Electrochemical Characterization of 316L Stainless Steel Coupons. Electrochemical impedance spectroscopy (EIS) and cyclic voltammetry were performed using a Princeton Applied Research Model 2273 potentiostat in a three-electrode electrochemical cell. The working electrode was the 316L stainless steel sample in a Teflon sample holder with 0.38 cm^2 exposed using a 7 mm diameter Viton O-ring, and a copper plate was used to make electrical contact with this sample. A platinum wire was used as a counter electrode, and all potentials were measured and reported relative to an Ag/AgCl reference electrode with a saturated KCl solution. A solution of 2 mM $Ru(NH_3)_6Cl_3$ in 0.1 M KCl was used to provide the electroactive species and the electrolyte for the cyclic voltammetry and EIS experiments, respectively. This enabled the EIS and cyclic voltammetry experiments to be performed sequentially, in the same apparatus, without changing the solution in the cell. Six samples were characterized for each type of coating, and the reported values are the averages over the six samples. For the cyclic voltammetry experiments, the potential was scanned from 0.05 to −0.4 V at scan rates of 250, 200, 150, 100, and 50 mV/s. The peak currents were determined from the cyclic voltammograms using Princeton Applied Research PowerCV software, and the electroactive area (A) was then calculated based on the slope of the Randles-Sevcik equation

$$I_P = (2.69\times10^5)n^{3/2}CD^{1/2}Av^{1/2}$$

where n is the number of electrons transferred in each redox reaction (in this case, n = 1), C is the analyte concentration, D is the analyte diffusion coefficient (9.78×10^{-6} cm^2/s), and v is the potential scan rate. The calculated electroactive area was divided by the exposed area of the working electrode, and expressed as a percentage. EIS experiments were performed at room temperature inside a Faraday cage. The magnitude and phase of the complex impedance were measured at 50 logarithmically distributed frequencies over the range of 55 kHz to 10 mHz, with an AC amplitude of 10 mV. The measured EIS data was then fit to the equivalent circuit found in the Supporting Information, Figure 14, using ZSimpWin version 3.21 software, and the system capacitance, C_s, which is a measure of the exposed surface area was extracted from the modeled data according to the following expression

$$C_s = \frac{1}{2\pi f_{max} R_p}$$

f_{max} is the frequency at which the imaginary component of impedance is maximized, and R_p is the equivalent circuit polarization resistance (see the Supporting Information, Table 1).

Assay for Determining Carbohydrate Attachment (ELLA). Each stainless steel surface was treated with a solution of 2% BSA in PBST (100 μL) and shaken (14 h, 5 °C). The surface was then removed and then incubated at room temperature with a solution of the lectin

Scheme 1. Illustration of the Procedure for Depositing a Silica Coating on Stainless Steel, Subsequent Surface Functionalization, and Detection of the Attached Antigen Using an Enzyme-Linked Lectin Assay (ELLA)[a]

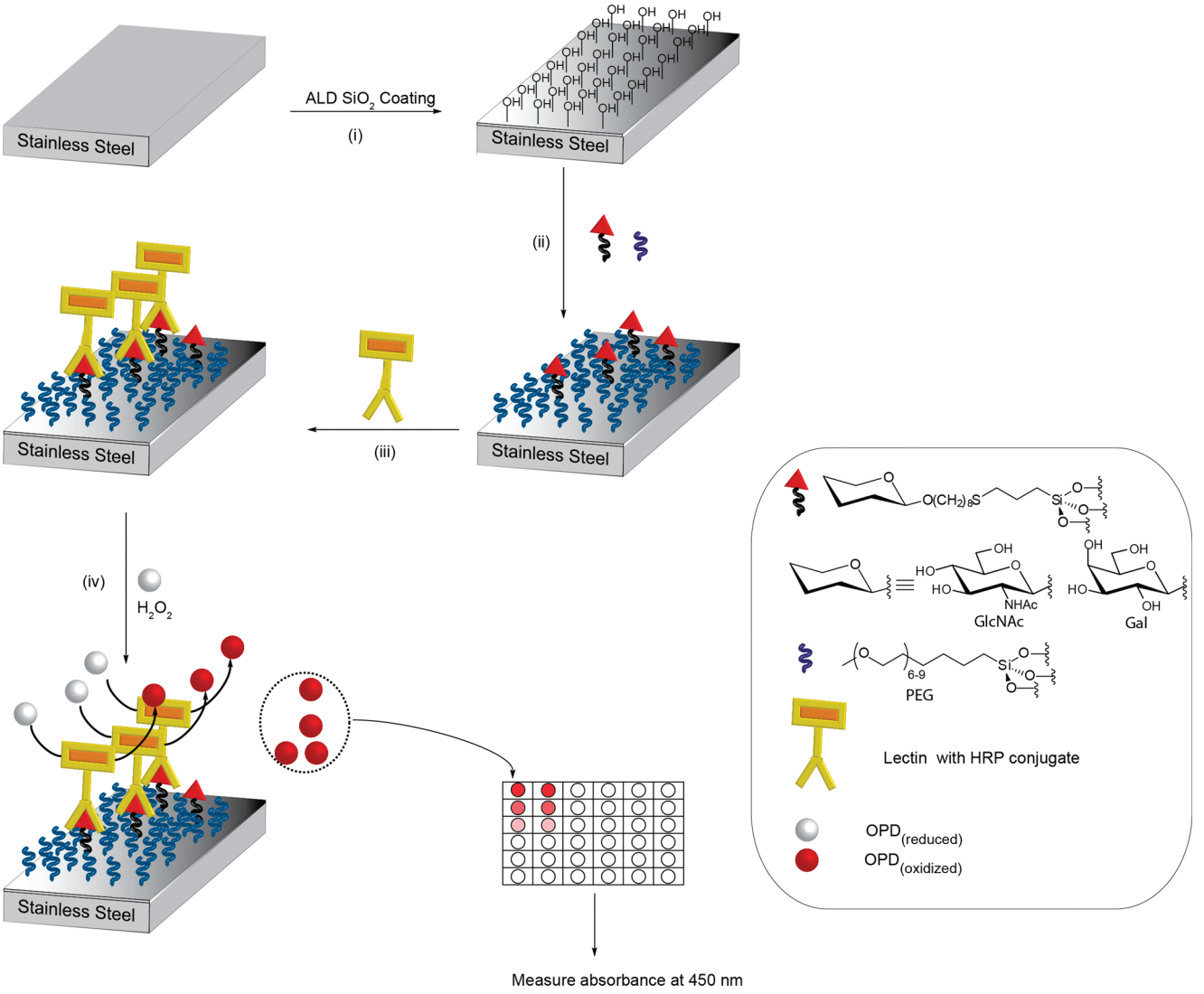

[a] (i) Formation of SiO_2 layer on 316L stainless steel via atomic layer deposition (ALD). (ii) Functionalization of SiO_2 surface with monosaccharide and PEG silanes. (iii) Treatment of functionalized SiO_2 coating with a carbohydrate specific lectin (WGA or PNA) containing a horseradish peroxidase (HRP) conjugate. (iv) Treatment with SigmaFast OPD; the horseradish peroxidase (HRP) of any bound lectin oxidizes the *o*-phenylenediamine, resulting in a colorimetric change.

peanut agglutinin (PNA) or wheat germ agglutinin (WGA)(0.01 mg/mL, 200 μL) in 2% BSA PBST for 2 h with shaking. The surface was thoroughly washed with PBST to remove unbound lectin and then treated with a solution of OPD (SIGMA*FAST* OPD, *o*-phenylenediamine) (500 μL, 1 h). The absorbance of an aliquot of this solution (200 μL) was measured at 450 nm.

RESULTS AND DISCUSSION

Our overall approach for preparing and characterizing carbohydrate-functionalized stainless steel surfaces integrated with (or without) PEG-based silanes is outlined in Scheme 1. A variety of techniques were explored to introduce the thin silica coating required for conjugation of the silane moieties, including dip coating, electrodeposition, and atomic layer deposition (ALD) [Scheme 1 (i)]. Once the appropriate route toward silica-coated stainless steel surfaces was identified (vide infra), the trialkoxysilane derivatives of the monosaccharides GlcNAc and Gal were then prepared and conjugated to the surface, often with polyethylene glycol (PEG)-based silanes that serve to control the average loading of the GlcNAc and Gal molecules on the surface [Scheme 1 (ii)], and for applications, reduce the propensity for non-specific surface adhesion.[74−77] These carbohydrate moieties bound to the stainless steel surface were then detected via a complementary enzyme-linked lectin assay (ELLA) [Scheme 1 (iii and iv)].

A high density of hydroxyl groups on the stainless steel surface must be induced in the first step of the functionalization strategy to allow efficient formation of controllable organic monolayers through alkoxysilane coupling reactions. Properly prepared, a silica coating that binds well to the stainless steel should satisfy this requirement. To determine the ideal silica deposition approach,

Scheme 2. Methods Used for Coating 316L Stainless Steel with Silica; Silica Layer Deposited via (i) Dip Coating, (ii) Electrodeposition, or (iii) Atomic Layer Deposition

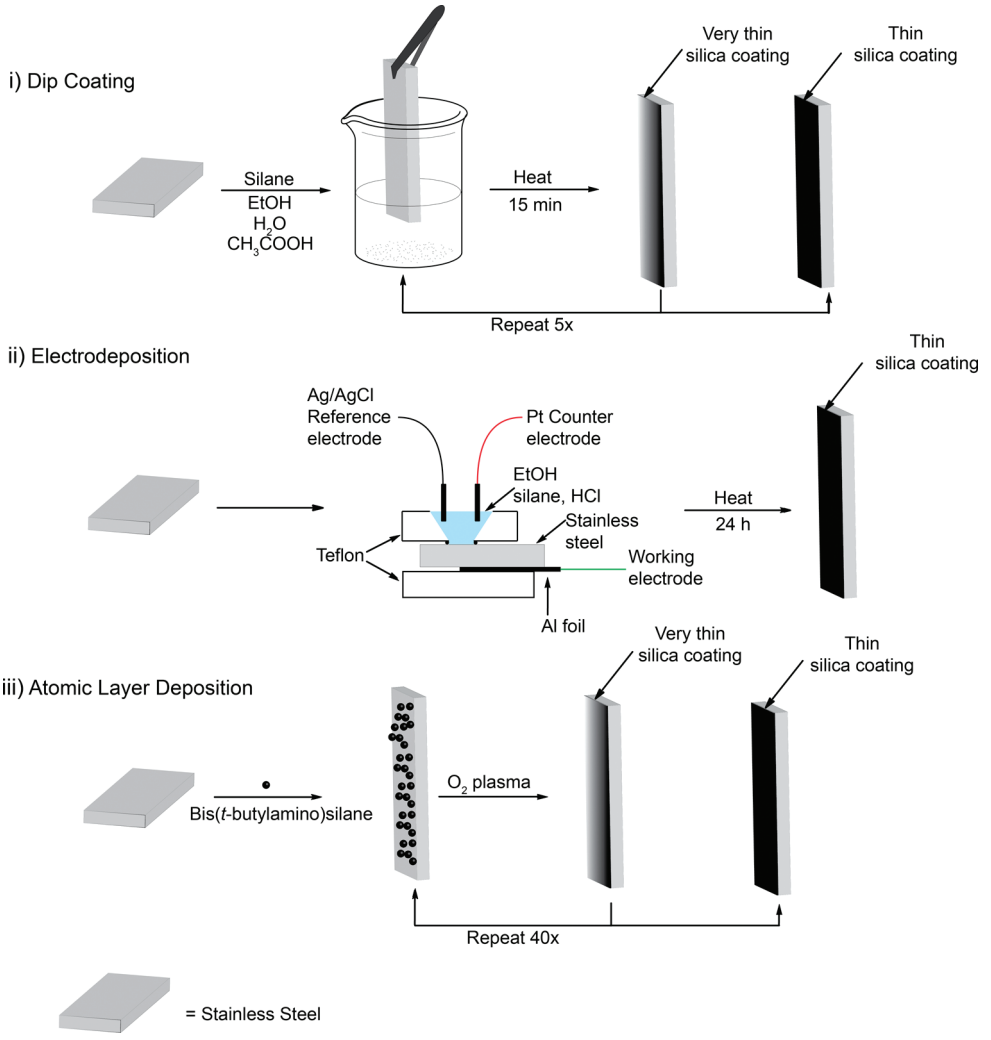

coatings were synthesized via three methods: (i) a sol−gel dip-coating procedure using neat and ethanolic solutions of tetraethylorthosilicate (TEOS), (ii) electrodeposition of a sol, and (iii) atomic layer deposition (ALD) (Scheme 2). Following the deposition of the silica layer, the carbohydrate- and PEG-based molecules were attached via standard alkoxysilane chemistry (Scheme 3 and 4).

As found in prior work, stainless steel functionalization has been traditionally fraught with challenges related to coverage.[46,60,64] Before addressing the surface density of the carbohydrate of interest, the surface coverage of the silica coating prepared via the three methods needed to be fully assessed. An ideal approach for stainless steel, because of its electrical properties, is to use electrochemistry as a probe to determine the coverage of the insulating silica layer. In this investigation the functionalized surface was used as a working electrode in a standard three-electrode cell and examined by cyclic voltammetry and electrochemical impedance spectroscopy (EIS). If the coverage of silica is complete and uniform, the stainless steel electrode will be electrically inactive because of the insulating nature of silica. Low electrical activity of the stainless steel also has important biocompatibility ramifications as metal biomedical implant thrombosis and fouling is thought to start with the non-specific binding of fibrinogen, followed by a one electron reduction to fibrin on the electropositive metal surface, starting a cascade of activation and adhesion of cells and platelets, together with clot formation.[12,13] Given the electrochemical nature of the cascade initiation, suppression of charge transfer events may act to lessen non-specific binding.

Figure 1 and Table 2 summarize the electrical characterization of silica coatings prepared via the methods described in Scheme 2. Representative cyclic voltammograms of clean and functionalized 316L stainless steel samples are shown in Figure 1(i). The effective electroactive area of an electrode can be calculated from a plot of cyclic voltammogram peak current versus scan rate$^{1/2}$ using the Randles−Sevcik equation (see the Supporting Information).[78] The calculated electroactive area was divided by the area of the working electrode exposed to the electrolyte and expressed as a percentage and the values (listed in Table 2) are averaged over six different samples. Considerable variation, up to 15%, even for clean stainless steel samples, was observed between samples in spite of the fact that

Scheme 3. Stainless Steel Surface Functionalization GlcNAc[a]

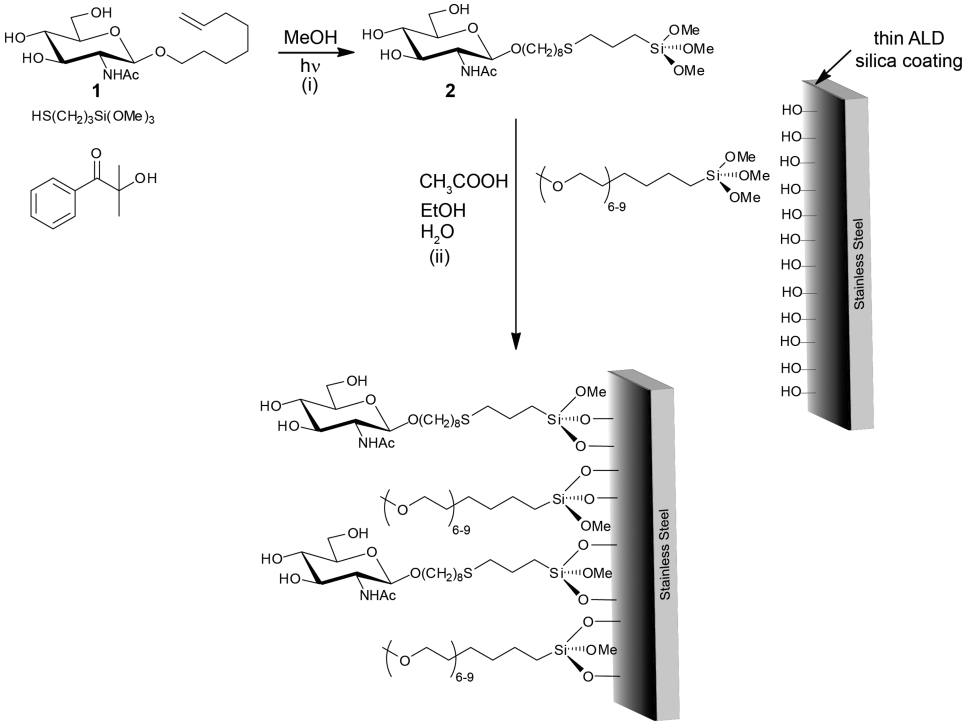

[a] (i) Trimethoxysilane functionalization of the 2-*N*-acetamido-2-deoxy-β-D-glucopyranoside **1**. (ii) Functionalization of a silica coated stainless steel surface via a dip-coating sol of a mixture of alkoxysilane PEG and the 2-*N*-acetamido-2-deoxy-β-D-glucopyranoside **2** in a predetermined ratio.

all were cut from the same 10 cm × 10 cm coupon; these variations can be attributed to differences in composition of the alloy and the resulting passivation layer.[79] As can be seen, the electroactive areas of the stainless steel samples depend considerably upon the functionalization method. For comparison, the calculated electroactive area of clean 316L stainless steel (sample A) is 83% (±5%), with the calculated electroactive area less than 100%, a fact attributed to the presence a native metal oxide passivation layer. The dip coating approaches show only small reductions in electroactive area, whereas the electrodeposition method led to a more substantial reduction, yielding an electroactive area of ∼18%. The ALD method, on the other hand, consistently produced coatings with electroactive area of 0% — complete electrical blocking within detection limits. The ability of even the thin (less than 15 nm thick) ALD SiO_2 coating to block all electrical transport to the stainless steel suggests that it is monolithic and nonporous, thus preventing the movement and transfer of ions, electrons, or other charge carriers.

Film thicknesses of the various layers measured by variable angle spectroscopic ellipsometry (VASE) are shown in Table 2, revealing little correlation between oxide thickness and electroactive area. Thickness values reported here represent those for which the best fit between the model and measured data were obtained. It should also be noted that the optical data for samples B−H are nearly indistinguishable from that of the reference, sample A. For these samples, variations in the reported thicknesses could be a result of uncertainties in the fitting routines or noise in the raw VASE data, and therefore, differences in the thicknesses cannot be attributed to the chemical processing with any degree of certainty. In other words, according to the VASE results, the dip coating methods did not appear to substantially thicken the dielectric coating beyond the native oxide already inherent to clean 316L stainless steel. In contrast, the electrodeposited coatings are thicker (up to ∼100 nm), although SEM (refer to the Supporting Information, Figure 14) and VASE collectively indicate that the coatings are porous and rough in comparison to clean 316L stainless steel. Although ALD-prepared SiO_2 interfaces all show complete blocking of electrical activity, these oxides are thin (less than 15 nm) and have morphologies similar to clean stainless steel precursor surfaces, indicating a pinhole-free coating.[50] Despite the thin coating, ALD-prepared films also obscure the X-ray photoelectron spectroscopy (XPS) signals from the buried alloy metals, further indicating that the coating is complete and nonporous (see the Supporting Information, Figure 15 and Table 2).

Figure 1(ii) shows the cyclic voltammograms of ALD SiO_2-coated stainless steel (sample K) and the alkoxysilane PEG-functionalized ALD coated stainless steel (sample L) on a smaller current scale. On this scale, it is apparent that the shape of the cyclic voltammograms of the ALD SiO_2 coated samples are different from that of the clean and alkoxysilane PEG functionalized stainless steel. The small amount of current measured in the cyclic voltammogram is due to capacitive charging of the system.[78] No reduction peak is present in the cyclic voltammograms for the ALD-functionalized silica-coated samples K or L, which indicates that no pinholes are present in this coating. If this were not the case, the $Ru(NH_3)_6^{3+}$ species would undergo reduction at the stainless steel working electrode, and thus to the sensitivity limit of our electrochemical apparatus, the 40 cycle ALD silica coating acts as an ideal blocking layer.

Scheme 4. Stainless Steel Surface Functionalization Gal[a]

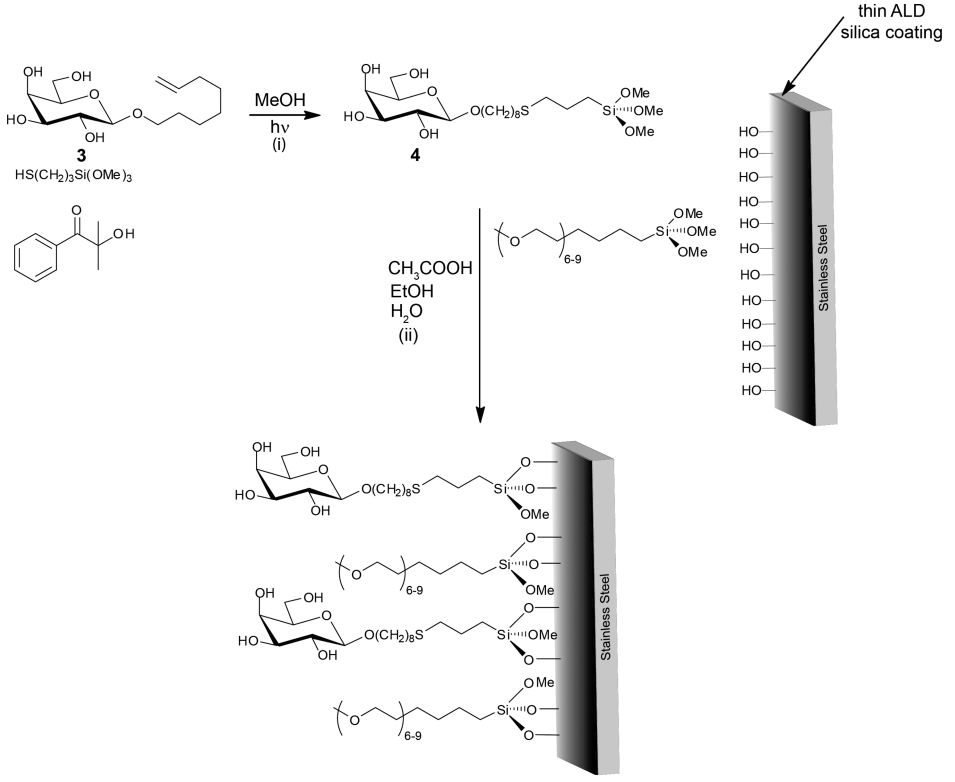

[a] (i) Trimethoxysilane functionalization of the β-D-galactopyranoside **3**. (ii) Functionalization of a silica coated stainless steel surface via a dip-coating sol of a mixture of alkoxysilane PEG and the β-D-galactopyranoside **4** in a predetermined ratio.

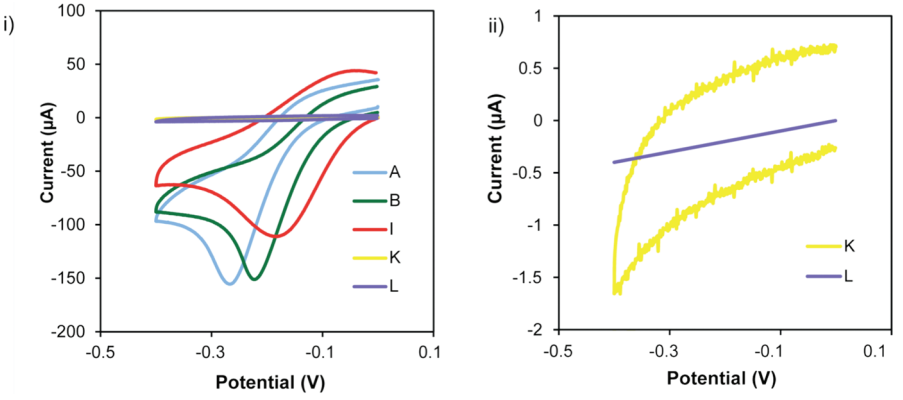

Figure 1. Cyclic voltammograms of clean and silica-coated stainless steel samples. For all plots, the blue line (A) denotes clean 316L SS; the green line (B) is sol−gel PEG-silane functionalized 316L SS; the red line (I) is 316 L SS functionalized with PEG-silane through electrodeposition; the yellow line (K) is 316L SS coated with 40 cycles of SiO_2 deposited via atomic layer deposition (ALD); and the purple line (L) is PEG-silane functionalized ALD deposited SiO_2 on 316L SS. (i) Cyclic voltammograms of A, B, I, K, and L over the voltage range 0.0 V to −0.4 V versus Ag/AgCl in saturated KCl solution with 2 mM $Ru(NH_3)_6Cl_3$. (ii) Expansion of cyclic voltammograms of K and L over the same voltage range.

Surface Functionalization. Monosaccharides **2** and **4** were synthesized from stable alkene terminated monosaccharides via a thiol−ene reaction as outlined in Schemes 3 and 4. The experimental procedures and spectroscopic data for each compound are included in the Supporting Information. The thiol−ene reaction is increasingly referred to as a "click" reaction because of its high specificity and yield.[80,81] The thiol−ene chemistry used to prepare both **2** and **4** produced minimal byproduct, and purification was achieved by washing the reaction mixture with hexanes. The preparation of carbohydrates with a trimethoxysilane linker enables the direct conjugation of these monosaccharides to any hydroxyl-rich surface, such as the silica-coated stainless steel used here.

The prepared ALD silica coated stainless steel surfaces were then functionalized by dip coating the sample in an acid-catalyzed sol of the desired silane, where either the 2-*N*-acetamido-2-deoxy-β-D-glucopyranoside (**2**) or the β-D-galactopyranoside (**4**) was conjugated directly to the silica-coated ALD stainless

Table 2. Electroactive Area (measured by CV), Film Thicknesses (as determined by variable angle spectroscopic ellipsometry (VASE), see the Supporting Information for further details), and Fraction of Fe, Cr, Mo, and Ni Metals (as observed by low resolution XPS) (refer to Surface Characterization in the Materials and Methods section for further details)

sample	electroactive area (%)	film thickness (nm)	% metal
reference			
(A) [clean 316L SS]	83 (5)	6	11 (3)
dip coating			
(B) [PEG-silane]	78 (10)	7	4 (1)
(C) [1,2-bis(trimethoxysilyl)ethane]	67 (5)	8	1.2 (0.6)
(D) [100% TEOS (no curing)]	79 (8)	6	3.0 (0.6)
(E) [100% TEOS]	75 (10)	8	6 (1)
(F) [1:1 TEOS:100% EtOH]	66 (8)	6	10 (1)
(G) [1:1 TEOS:95% EtOH/AcOH]	68 (8)	7	6 (2)
(H) [1:1 TEOS:95% EtOH]	73 (8)	8	8 (2)
electrodeposition			
(I) [electrodeposited PEG-silane]	54 (9)	40	0.7 (0.4)
(J) [electrodeposited TEOS]	18 (14)	103	2(2)
atomic layer deposition			
(K) [ALD SiO_2]	0 (0)	11	0.7 (0.3)
(L) [ALD SiO_2-PEG-silane]	0 (0)	23	0.03 (0.04)

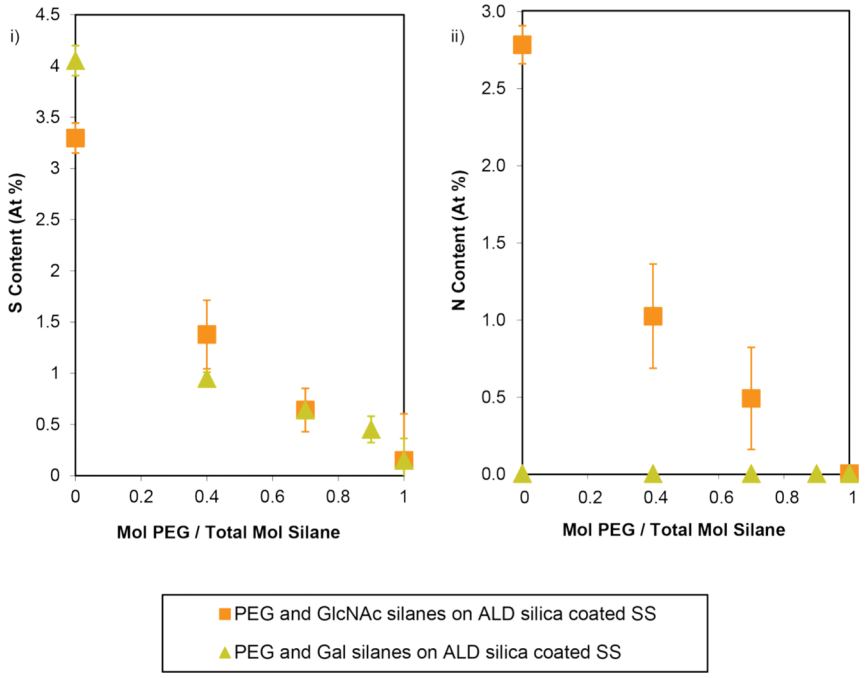

Figure 2. Atomic % of (i) nitrogen and (ii) sulfur determined via low resolution XPS of 40 cycle ALD silica-coated 316L stainless steel with mixtures of GlcNAc or Gal and PEG silanes.

steel surface. In the sol, the methoxy groups of the silane are hydrolyzed to silanols, which enables the monosaccharide silane to hydrogen bond to the surface.[82,83] Upon removal from the sol, the sample is cured, resulting in condensation to form covalent silicon−oxygen−silicon bonds.[82] Importantly, the silanol groups do not react with the hydoxyl groups of the unprotected monosaccharides. This lack of cross-reactivity is likely due to the low pH of the sol−gel deposition solution, essentially hydrolyzing any silyl ethers formed (the acid lability of silyl ethers is well documented).[84] The detection of sulfur in the XPS of substrates reacted with either the GlcNAc or Gal silanes, and the detection of nitrogen in the substrates reacted with GlcNAc silanes, is indicative of the presence of attached silanes to the 40-cycle ALD silica-coated stainless steel (shown in Figure 2).

To further increase the functionality and versatility of the surface chemistry, mixed monolayers of PEG and the monosaccharide were examined. For different applications, control over average saccharide spacings, and reduction of non-specific protein binding could be important.[75−77] Mixed monolayers of different alkoxysilanes are known, and can be prepared through

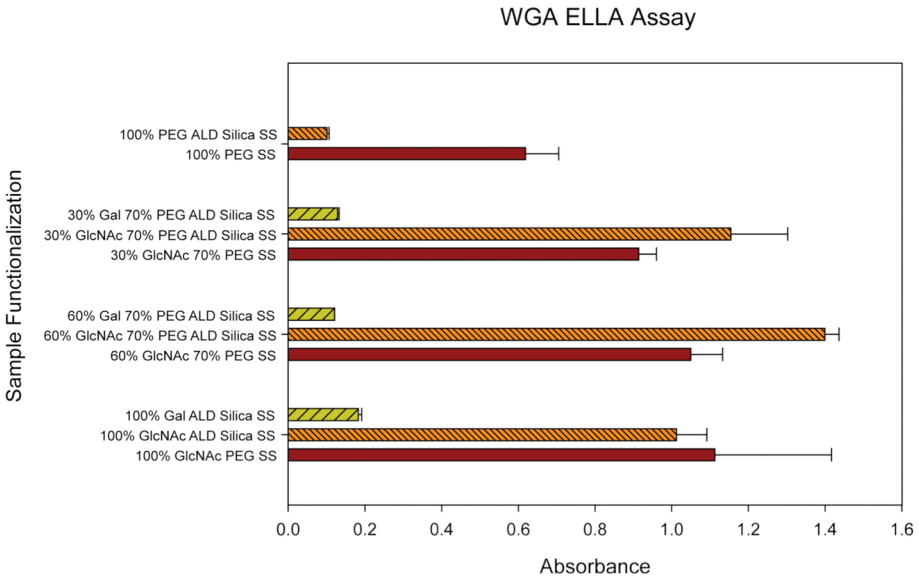

Figure 3. Wheat germ agglutinin (WGA) GlcNAc (**2**) specific ELLA assay conducted on glycan-functionalized stainless steel coupons.

conjugation of a solution of the silane precursors with the desired ratio.[74] Therefore, a sol−gel containing a mixture of alkoxysilane PEG and the trimethoxysilane monosaccharide derivatives was expected to result in a functionalized silica surface with approximately the same ratio of PEG and monosaccharide moieties as the surface chemistry is similar. As shown in Figure 2, mixtures of the PEG and GlcNAc silane were reacted with silica-coated stainless steel, ranging from 100% PEG to 100% GlcNAc. Monitoring the sulfur and nitrogen content of the films by XPS showed that there is a decrease in the presence of these two elements (derived from the GlcNAc) as the PEG/total silane ratio decreases. FTIR transmission spectroscopy of a high-surface-area model substrate, oxidized porous silicon, functionalized with the same sol−gel solutions as the stainless steel substrates reveal a similar trend: the GlcNAc amide peak disappears with increasing PEG incorporation, and simultaneously the intensity of C−O−C peaks increases (see the Supporting Information). As can be seen in Figure 2(i), the galactose (Gal)-functionalized surfaces exhibit the same trend in surface sulfur content as the PEG/total silane ratio is changed. The XPS data in Figure 2(ii) also show no detectable nitrogen on the surfaces of samples where the monosaccharide incorporated was Gal, as one would expect for a carbohydrate that does not contain nitrogen. These observations confirm that there is a correlation between the ratio of silanes used in the sol−gel functionalization solution and the resulting surface functionalization.

Enzyme-Linked Lectin Assays (ELLA) for Specific Detection of Glucopyranoside-Functionalized Surfaces. One of the challenges in developing this methodology for conjugating carbohydrates to stainless steel surfaces has been the accompanying need for development of new techniques to detect these bound species. ELISA (enzyme-linked immunosorbent assay) has been used to detect carbohydrates immobilized on other surfaces such as glass or plastic.[85,86] Traditionally, an ELISA detects bound carbohydrates first by treating an antigen functionalized surface with an antibody specific for the carbohydrate. The antibody is then linked to an enzyme capable of producing a detectable signal change. The replacement of an antibody with a lectin results in an assay that is formally not an ELISA; typically these assays are referred to as a modified ELISA or an ELLA (enzyme-linked lectin assay). The ELLA used in this study is outlined in Scheme 1 (parts iii + iv). Two carbohydrates were selected based upon the availability of the appropriate peroxidase-conjugated lectins. To this end, wheat germ agglutinin (WGA) and peanut agglutinin (PNA) were selected based on their ability to recognize *N*-acetyl-β-D-glucosamine and β-D-galactose, respectively. WGA binds to GlcNAc; methyl β-D-GlcNAc has an IC_{50} of 10 mM.[87] The binding of PNA to Gal is a weaker interaction; the IC_{50} for methyl β-D-galactopyranoside is 80 mM.[88]

Two sets of 40 cycle ALD silica-coated stainless steel samples and one set of uncoated stainless steel samples were utilized and are detailed in Table 1. The uncoated stainless steel samples were utilized in order to provide a comparison to the ALD silica-coated stainless steel surfaces. Each surface, after appropriate blocking to minimize non-specific binding, was washed to remove excess and non-specifically bound lectin, followed by treatment with a soluble peroxidase indicator (OPD). The absorbance of the resulting solution was measured at 450 nm to provide a semi-quantitative indication as to the quantity of lectin bound to the surface.

The data in Figures 3 and 4 indicate selective binding of each carbohydrate to the complementary lectin. WGA is capable of binding to GlcNAc, even when the carbohydrate density is low (30% GlcNAc, 70% PEG), as can be seen from Figure 3. Binding of the WGA to the Gal moiety, as one would expect, is minimal since they are not complementary. This binding of WGA to GlcNAc and not to Gal, combined with the absence of binding to the 100% PEG control, conclusively demonstrates that this binding is a glycan-specific interaction. The 100% PEG ALD silica SS sample (Figure 3) showed low levels of non-specific binding as one would expect whereas WGA showed some binding to the 100% PEG SS sample (Figure 3), as indicated by the increased absorbance value. The higher level of non-specific binding is attributed to insufficient PEG coverage on the directly functionalized stainless steel, pointing to the conclusion that the ALD silica layer is an excellent base for functionalization.

Binding of PNA agglutinin to Gal (Figure 4) was apparent only at higher Gal concentrations when compared to the binding of WGA to GlcNAc. The weaker binding of Gal to PNA, when

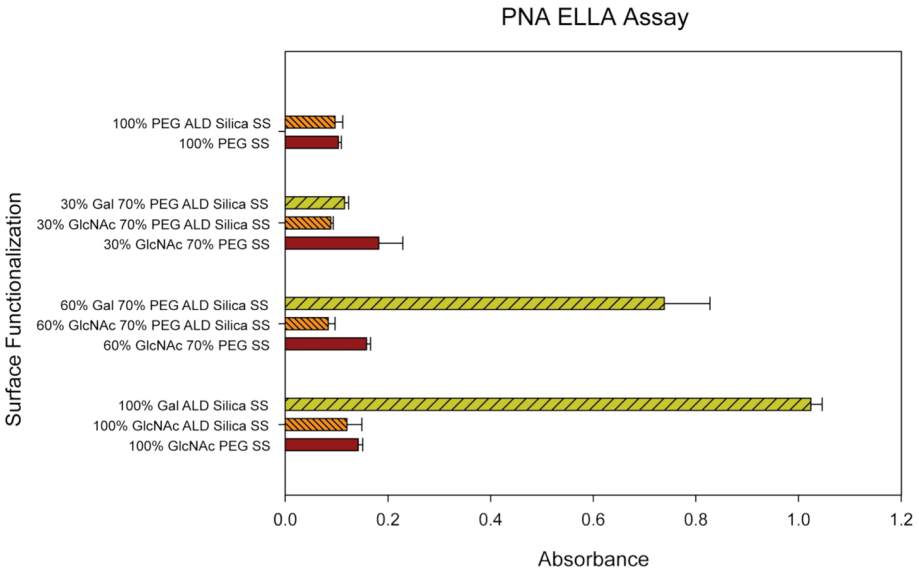

Figure 4. Peanut agglutinin (PNA) Gal (**4**) specific ELLA assay conducted on glycan-functionalized stainless steel coupons.

compared to GlcNAc and WGA, is one possible explanation for this observation. It could be inferred that at higher carbohydrate densities, there would be sufficient multivalent bindings between PNA and the Gal residue attached to ensure that the lectin is not washed away during the rinse steps. This threshold effect was first reported by Orr and co-workers in their studies on ConA binding to cholesterol mannose derivatives.[89] The absence of binding to GlcNAc and the 100% PEG ALD silica SS control conclusively demonstrates that this binding is glycan-specific and not caused by non-specific binding to either the surface or other glycans.

Lectins typically have multiple binding sites and rely on multivalent interactions to affect binding: WGA is a dimeric protein with a total of eight binding sites.[90] In contrast, PNA is a dimer of dimers, with each subunit possessing a single binding site.[91] As lectin−carbohydrate interactions are generally low affinity, multivalent interactions become an important factor, as is particularly evident in Figure 4 where at 30% Gal concentration the density is insufficient to result in detectable binding. The higher avidity of WGA-GlcNAc interactions in combination with the affinity of each interaction is a likely explanation for the ability of WGA to bind to GlcNAc at lower densities.

Glycan density is an important consideration for any glycan-functionalized surface that is designed to interact with a biological system.[92] A greater concentration of glycan does not necessarily result in greater binding, as evident in Figure 3 where maximum binding is achieved at 30% GlcNAc density, indicated by the plateau in absorbance values. In this case, at best the excess glycan is wasted and at worst the excess glycan is detrimental to lectin binding. The molecules investigated here (GlcNAc and Gal moieties) are relatively easy to prepare and inexpensive; therefore, wastage of the materials is not of significant concern. However, in many other cases, wastage of more complex glycans, prepared through lengthy synthetic routes, is undesirable. Thus, careful attention should be paid to ensuring that optimum glycan density is obtained, to maximize both the biological effect and reduce substrate wastage.

CONCLUSIONS

An ultrathin coating of silica was prepared on 316L stainless steel through atomic layer deposition. To the limits of sensitivity of the apparatus, the 40 cycle ALD silica coating was completely electrically blocking and nonporous, likely due to the ALD coating formation mechanism. Trialkoxysilane derivatives of two monosaccharides (**2** and **4**) were prepared via a rapid and efficient thiol−ene coupling, which enabled straightforward functionalization of the silica-coated stainless steel surface. Alongside XPS detection, the presence and biological availability of monosaccharides **2** and **4** were confirmed by ELLA, utilizing the complementary lectins WGA and PNA.

These biological tests not only confirmed the presence of the glycans on the stainless steel surface but also highlighted the importance of controlling the glycan density. Minimal glycan density is required to ensure that sufficient avidity is obtained, as was evident in the case of WGA−GlcNAc interactions (Figure 3). The ability to control the glycan density using straightforward mixed alkoxysilane coupling coupling chemistry, combined with the effectiveness of ALD coatings, provide a new technique for the preparation of glycan-functionalized stainless steel surfaces.

ASSOCIATED CONTENT

Supporting Information. Twenty-nine pages describing porous silicon synthesis and characterization, and additional details and data regarding electrochemical surface functionalization, carbohydrate synthesis, and ALD. This material is available free of charge via the Internet at http://pubs.acs.org.

AUTHOR INFORMATION

Corresponding Author

*E-mail: tlowary@ualberta.ca (T.L.L); jburiak@ualberta.ca (J.M.B.).

ACKNOWLEDGMENT

Funding for this work was obtained via a CIHR team grant (RMF 92091), an NSERC/CIHR CHRP grant (CHRPJ350946-08), and

NRC-NINT. Andrew Bonifas is thanked for discussions on determinations of electroactive area and electrochemical impedance spectroscopy. The Alberta Centre for Surface Engineering and Science (ACSES) is thanked for XPS analysis. Bryan Szeto, Dr. Richard McCreery and the NINT Cleanroom staff are thanked for use of the ALD. Additionally, NSERC and Alberta Innovates—Technology Futures are gratefully acknowledged for scholarships to A.M.S.

REFERENCES

(1) Köster, R.; Vieluf, D.; Kiehn, M.; Sommerauer, M.; Kähler, J.; Baldus, S.; Meinertz, T.; Hamm, C. W. *Lancet* **2000**, *365*, 818–826.
(2) O'Brien, B.; Carrol, W. *Acta Biomater.* **2009**, *5*, 945–958.
(3) Navarro, M.; Michiardi, A.; Castaño, O.; Planell, J. A. *J. R. Soc. Interface* **2008**, *5*, 1137–1158.
(4) Long, M.; Rack, H. J. *Biomaterials* **1998**, *19*, 1621–1639.
(5) Mani, G.; Feldman, M. D.; Patel, D.; Agrawal, C. M. *Biomaterials* **2007**, *28*, 1689–1710.
(6) Gotman, I. *J. of Endourology* **1997**, *11*, 383–389.
(7) Zilberman, M.; Eberhart, R. C. *Annu. Rev. Biomed. Eng.* **2006**, *8*, 153–180.
(8) Frankel, G. S. *J. Electrochem. Soc.* **1998**, *145*, 2186–2198.
(9) Diaz, M.; Sevilla, P.; Galán, A. M.; Escolar, G.; Engel, E.; Gil, F. J. *J. Biomed. Mater. Res., Part B* **2008**, *87B*, 555–561.
(10) Hallab, N.; Jacobs, J. J.; Black, J. *Biomaterials* **2000**, *21*, 1301–1314.
(11) Hanawa, T. *Mater. Sci. Eng., C* **2004**, *24*, 745–752.
(12) *Engineering Materials for Biomedical Applications*, 1st ed.; World Scientific Publishing Co. Pte. Ltd.: Singapore, 2004; Vol. 1, p 352.
(13) *Service Characteristics of Biomedical Materials and Implants*; Imperial College Press: London, 2004; Vol. 3, p 242.
(14) Kukreja, N.; Onuma, Y.; Daemen, J.; Serruys, P. W. *Pharmacol. Res.* **2008**, *57*, 171–180.
(15) Sydow-Plum, G.; Tabrizian, M. *Mater. Sci. Technol.* **2008**, *24*, 1127–1143.
(16) Bailey, S. R. *J. Intervention Cardiol.* **2009**, *22*, S3–S17.
(17) Lewis, A. L.; Furze, J. D.; Small, S.; Robertson, J. D.; Higgins, B. J.; Taylor, S.; Ricci, D. R. *J. Biomed. Mater. Res.* **2002**, *63*, 699–705.
(18) Lewis, A. L.; Tolhurst, L. A.; Stratford, P. W. *Biomaterials* **2002**, *23*, 1697–1706.
(19) Danzi, G. B.; Capuano, C.; Sesana, M.; Di Blasi, A.; Predolini, S.; Antoniucci, D. *Catheter. Cardiovasc. Intervent.* **2002**, *55*, 157–162.
(20) vom Dahl, J.; Haager, P. K.; Grube, E.; Gross, M.; Beythien, C.; Kromer, E. P.; Cattelaens, N.; Hamm, C. W.; Hoffmann, R.; Reineke, T.; Klues, H. G. *Am. J. Cardiol.* **2002**, *89*, 801–805.
(21) Airoldi, F.; Colombo, A.; Tavano, D.; Stankovic, G.; Klugmann, S.; Paolillo, V.; Bonizzoni, E.; Briguori, C.; Carlino, M.; Montorfano, M.; Liistro, F.; Castelli, A.; Ferrari, A.; Sgura, F. A.; Di Mario, C. *Am. J. Cardiol.* **2004**, *93*, 474–477.
(22) Sgura, F. A.; Di Mario, C.; Liistro, F.; Montorfano, M.; Colombo, A.; Grube, E. *Herz* **2002**, *27*, 514–517.
(23) Di Mario, C.; Grube, E.; Nisanci, Y.; Reifart, N.; Colombo, A.; Rodermann, J.; Muller, R.; Umman, S.; Liistro, F.; Montorfano, M.; Alt, E. *Int. J. Cardiol.* **2004**, *95*, 329–331.
(24) Windecker, S.; Simon, R.; Lins, M.; Klaus, V.; Eberli, F. R.; Roffi, M.; Pedrazzini, G.; Moccetti, T.; Wenaweser, P.; Togni, M.; Tüller, D.; Zbinden, R.; Seiler, C.; Mehilli, J.; Kastrati, A.; Meier, B.; Hess, O. M. *Circulation* **2005**, *111*, 2617–2622.
(25) Carrié, D.; Lefevre, t.; Cherradi, R.; Dumas, P.; Elbaz, M.; Finet, G.; Puel, J.; Morice, M. C. *J. Intervent. Cardiol.* **2007**, *20*, 381–388.
(26) Wieneke, H.; Dirsch, O.; Sawitowski, T.; Gu, Y. L.; Brauer, H.; Dahmen, U.; Fischer, A.; Wnendt, S.; Erbel, R. *Catheter. Cardiovasc. Intervent.* **2003**, *60*, 399–407.
(27) Lo, K. H.; Shek, C. H.; Lai, J. K. L. *Mater. Sci. Eng., R* **2009**, *65*, 39–104.
(28) Schmuki, P. *J. Solid State Electrochem.* **2002**, *6*, 145–164.
(29) Suzuki, O. In *Encyclopedia of Surface and Colloid Science*; Somasundaran, P., Ed; Taylor and Francis: New York, 2006; Vol. 1, p 185.
(30) Shih, C.-C.; Shih, C.-M.; Chen, Y.-L.; Su, Y.-Y.; Shih, J.-S.; Kwok, C.-F.; Lin, S.-J. *J. Biomed. Mater. Res.* **2001**, *57*, 200–207.
(31) Shrivastava, R.; Upreti, R. K.; Seth, P. K.; Chaturvedi, U. C. *FEMS Immunol. Med. Microbiol.* **2002**, *34*, 1–7.
(32) Haïdopoulos, M.; Turgeon, S.; Sarra-Bournet, C.; Laroche, G.; Mantovani, D. *J. Mater. Sci.: Mater. Med.* **2006**, *17*, 647–657.
(33) Doran, A.; Law, F. C.; Allen, M. J.; Rushton, N. *Biomaterials* **1998**, *19*, 751–759.
(34) Pazzaglia, U. E.; Minoia, C.; Ceciliani, L.; Riccardi, C. *Acta Orthopaedica Scandinavica* **1983**, *54*, 574–579.
(35) Okazaki, Y.; Gotoh, E. *Corros. Sci.* **2008**, *50*, 3429–3438.
(36) Cadosch, D.; Chan, E.; Gautschi, O. P.; Filgueira, L. *J. Biomed. Mater. Res., Part A* **2009**, *91A*, 1252–1262.
(37) Hansi, C.; Arab, A.; Rzany, A.; Ahrens, I.; Bode, C.; Hehrlein, C. *Catheterization Cardiovasc. Intervention* **2009**, *73*, 488–496.
(38) Roach, P.; Eglin, D.; Rohde, K.; Perry, C. C. *J. Mater. Sci: Mater. Med.* **2007**, *18*, 1263–1277.
(39) Ratner, B. D.; Bryant, S. J. *Annu. Rev. Biomed. Eng.* **2004**, *6*, 41–75.
(40) Variola, F.; Vetrone, F.; Richert, L.; Jedrzejowski, P.; Yi, J.-H.; Zalzal, S.; Clair, S.; Sarkissian, A.; Perepichka, D. F.; Wuest, J. D.; Rosei, F.; Nanci, A. *Small* **2009**, *5*, 996–1006.
(41) Anand, G.; Zhang, F.; Linhardt, R. J.; Belfort, G. *Langmuir* **2011**, *27*, 1830–1836.
(42) Thevenot, P.; Hu, W.; Tang, L. *Curr. Top. Med. Chem.* **2008**, *8*, 270–280.
(43) Shahryari, A.; Azari, F.; Vali, H.; Omanovic, S. *Acta Biomater.* **2010**, *6*, 695–701.
(44) Shih, C.-C.; Shih, C.-M.; Su, Y.-Y.; Chang, M.-S.; Lin, S.-J. *Appl. Surf. Sci.* **2003**, *219*, 347–362.
(45) Shih, C.-C.; Shih, C.-M.; Su, Y.-Y.; Su, L. H. J.; Chang, M.-S.; Lin, S.-J. *Thromb. Res.* **2003**, *111*, 103–109.
(46) Shih, C.-C.; Shih, C.-M.; Chou, K.-Y.; Lin, S.-J.; Su, Y.-Y. *J. Biomed. Mater. Res. Part A* **2007**, *80A*, 861–873.
(47) Bertrand, N.; Drévillon, B.; Gheorghiu, A.; Sénémaud, C.; Martinu, L.; Klemberg-Sapieha, J. E. *J. Vac. Sci. Technol., A* **1998**, *16*, 6–12.
(48) Kang, C.-K.; Lee, Y., -Sik *J. Mater. Sci.: Mater. Med.* **2007**, *18*, 1389–1398.
(49) Yuan, S. J.; Pehkonen, S. O.; Ting, Y. P.; Neoh, K. G.; Kang, E. T. *Langmuir* **2010**, *26*, 6728–6736.
(50) Jussila, P.; Ali-Löytty, H.; Lahtonen, K.; Mirsimäki, M.; Valden, M. *Surf. Interface Anal.* **2010**, *42*, 157–164.
(51) Singh, R.; Dahotre, N. B. *J. Mater. Sci.: Mater. Med.* **2007**, *18*, 725–751.
(52) Mahapatro, A.; Johnson, D. M.; Patel, D. N.; Feldman, M. D.; Ayon, A. A.; Agrawal, C. M. *Curr. Top. Med. Chem.* **2008**, *8*, 281–289.
(53) Ruan, C.-M.; Bayer, T.; Meth, S.; Sukenik, C. N. *Thin Solid Films* **2002**, *419*, 95–104.
(54) Shaulov, Y.; Okner, R.; Levi, Y.; Tal, N.; Gutkin, V.; Mandler, D.; Domb, A. J. *ACS Appl. Mater. Interfaces* **2009**, *1*, 2519–2528.
(55) Ignatova, M.; Voccia, S.; Gabriel, S.; Gilbert, B.; Cossement, D.; Jérôme, C. *Langmuir* **2009**, *25*, 891–902.
(56) Ignatova, M.; Voccia, S.; Gilbert, B.; Markova, N.; Cossement, D.; Gouttebaron, R.; Jérôme, R.; Jérôme, C. *Langmuir* **2006**, *22*, 255–262.
(57) Gabriel, S.; Jérôme, R.; Jérôme, C. *Prog. Polym. Sci.* **2010**, *35*, 113–140.
(58) Zheludkevich *J. Mater. Chem.* **2005**, *15*, 5099–5111.
(59) Gallardo, J.; Galliano, P.; Durán, A.; Gómez Coedo, A.; Dorado, T.; Garcia, C.; Ceré, S. *J. Mater. Chem.* **2004**, *14*, 2282–2290.
(60) Meth, S.; Sukenik, C. N. *Thin Solid Films* **2003**, *425*, 49–58.
(61) Yuan, S.; Wan, D.; Liang, B.; Pehkonen, S. O.; Ting, Y. P.; Neoh, K. G.; Kang, E. T. *Langmuir* **2011**, *27*, 2761–2774.
(62) Vreuls, C.; Zocchi, G.; Thierry, B.; Garitte, G.; Griesser, S. S.; Archambeau, C.; Weerdt, C. V. d.; Martial, J.; Griesser, H. *J. Mater. Chem.* **2010**, *20*, 8092–8098.

(63) Caro, A.; Humblot, V.; Méthivier, C.; Minier, M.; Salmain, M.; Pradier, C.-M. *J. Phys. Chem. B* **2009**, *113*, 2101–2109.
(64) Kaufmann, C. R.; Mani, G.; Marton, D.; Johnson, D. M.; Agrawal, C. M. *Biomed. Mater.* **2010**, *5*, 1–10.
(65) Mahapatro, A.; Johnson, D. M.; Patel, D. N.; Feldman, M. D.; Ayon, A. A.; Agrawal, C. M. *Langmuir* **2006**, *22*, 901–905.
(66) Adenier, A.; Bernard, M.-C.; Chehimi, M. M.; Cabet-Deliry, E.; Desbat, B.; Fagebaume, O.; Pinson, J.; Podvorica, F. *J. Am. Chem. Soc.* **2001**, *123*, 4541–4549.
(67) Gabriel, S.; Dubruel, P.; Schacht, E.; Jonas, A. M.; Gilbert, B.; Jérôme, R.; Jérôme, C. *Angew. Chem., Int. Ed.* **2005**, *44*, 5505–5509.
(68) Cécius, M.; Jérôme, C. *Prog. Org. Coat.* **2011**, *70*, 220–223.
(69) Melo-Júnior, M. R.; Cavalcanti, C. d. L. B.; de Pontes-Filho, N. T.; de Cavalho, L. B.; Beltrão, E. I. C. *Int. J. Morphol.* **2008**, *26*, 967–972.
(70) Kannan, S.; Lakki, R. A.; Jayakumar, K.; Steven, A. H.; Taralakshimi, V. V.; Chandramohan, S.; Balakrishan, R.; Schmidt, C.; Halagowder, D. *Mol. Cancer* **2003**, *2*, 38.
(71) Molin, K.; Fredman, P.; Svennerholm, L. *FEBS Lett.* **1986**, *205*, 51–55.
(72) El-Boubbou, K.; Zhu, D. C.; Vasileiou, C.; Borhan, B.; Prosperi, D.; Li, W.; Huang, X. *J. Am. Chem. Soc.* **2010**, *132*, 4490–4499.
(73) Okner, R.; Domb, A. J.; Mandler, D. *New J. Chem.* **2009**, *33*, 1596–1604.
(74) Lim, J. A.; Cho, J. H.; Jang, Y.; Han, J. T.; Cho, K. *Thin Solid Films* **2006**, *515*, 2079–2084.
(75) Jo, S.; Park, K. *Biomaterials* **2000**, *21*, 605–616.
(76) Lee, J. H.; Lee, H. B.; Andrade, J. D. *Prog. Polym. Sci.* **1995**, *20*, 1043–1079.
(77) Vermette, P.; Meaagher, L. *Colloids Surf., B* **2003**, *28* (2−3), 153–198.
(78) Bard, A. J.; Faulkner, L. R., *Electrochemical Methods Fundamentals and Applications*, 2nd ed.; John Wiley & Sons: New York, 2001; p 833.
(79) Hryniewicz, T.; Rokosz, K.; Filippi, M. *Materials* **2009**, *2*, 129–145.
(80) Dondoni, A. *Angew. Chem., Int. Ed.* **2008**, *47*, 8995–8997.
(81) Hoyle, C. E.; Bowman, C. N. *Angew. Chem., Int. Ed.* **2010**, *49*, 1540–1573.
(82) van Ooij, W. J.; Zhu, D.; Stacy, M.; Seth, A.; Mugada, T.; Gandhi, J.; Puomi, P. *Tsinghua Sci. & Tech.* **2005**, *10*, 639–664.
(83) Zhang, F.; Kang, E. T.; Neoh, K. G.; Wang, P.; Tan, K. L. *Biomaterials* **2001**, *22*, 1541–1548.
(84) Greene, T. W.; Wuts, P. G. M. *Protective Groups in Organic Synthesis*, third ed.; John Wiley & Sons: New York, 1999.
(85) Engvall, E.; Perlmann, P. *Immunochemistry* **1971**, *8*, 871–874.
(86) Van Weemen, B. K.; Schuurs, A. H. W. M. *FEBS Lett.* **1971**, *15*, 232–236.
(87) Allen, K. A.; Neuberger, A.; Sharon, N. *Biochem. J.* **1973**, *131*, 155–162.
(88) Lotan, R.; Skutelsky, E.; Sharon, N. *J. Biol. Chem.* **1975**, *25*, 8518–8523.
(89) Orr, G. A.; Rando, R. R.; Bangerter, F. W. *J. Biol. Chem.* **1979**, *254*, 4721–4725.
(90) Wright, C. S. *J. Biol. Chem.* **1992**, *267*, 14345–14352.
(91) Natchair, S. K.; Suguna, K.; Surolai, A.; Vijayan, M. *Crystallogr. Rev.* **2007**, *13*, 3–28.
(92) Dam, T. K.; Brewer, C. F. *Glycobiology* **2010**, 270–279.